Rev.Adv.Mater.Sci. 15(2007) 173-178

OPTICAL AND ELECTRICAL PROPERTIES OF SPUTTERED Zr-Si-N THIN FILMS: FROM SOLID SOLUTION TO NANOCOMPOSITE

C.S. Sandu, F. Medjani and R. Sanjinés

Institute of Physics of Complex Matter, EPFL, CH-1015 Lausanne, Switzerland

Received: January 22, 2007

Abstract. DC reactive magnetron sputtering was used for the deposition of Zr-Si-N thin films. Four series of samples have been deposited at various substrate temperatures T_S: room temperature (RT), 240 °C, 440 °C, and 640 °C. The total pressure was 0.6 Pa. Depending on T_S, different N_2 partial pressures are required for obtaining nearly stoichiometric ZrN films. The nitrogen partial pressure was kept constant for each series at 5%, 12.5%, 37.5%, and 65%, respectively. Si content (C_{Si}) was varied in each series by changing the power applied on the Si target, whereas that on Zr target was kept constant. Besides the standard characterization techniques, electrical resistivity measurements have been performed between 20 and 300K. The results of theoretical fitting using the grain boundary scattering model show that the transport properties change with Si addition from a moderated damping regime to a strong damping regime. The optical properties of the Zr-Si-N films with $C_{Si} \leq 10$ at.% can be well explained by straight forward modeling of their dielectric functions by a set of Drude-Lorentz oscillators. In this model, the Drude damping factor Γ_p (or time relaxation of the free carriers) is mainly related to the film morphology, i.e. the crystallite size and the nature of the grain boundary barrier. The electron transmission probability G (obtained from fitting of resistivity measurements), the Si coverage on the ZrN grain surfaces (obtained from structural model calculation) and the Drude damping factor Γ_p (obtained from fitting the dielectric function) are well correlated.

1. INTRODUCTION

By addition of Si to a binary transition metal nitride TMN (e.g. TiN, ZrN, NbN), hardness, thermal stability and chemical inertness of films have been considerably improved [1-5]. Even in small quantity, this third element plays a decisive role in the modification of chemical bonding, morphology and structure of the coating. The formation of a nanocomposite (crystallites of TMN + amorphous SiN_y) [2] and/or a solid solution single phase material [6,7] are possible by varying the deposition conditions. A 3-step model for the film formation based on experimental results has been recently proposed for the particular case of Nb-Si-N ternary system deposited by DC magnetron sputtering [8,9] and then extent for Ti-Si-N, Zr-Si-N, Cr-Si-N systems [10,11]. The model presents the evolution of the film structure as a function of Si content. For low Si content (Domain1) the Si atoms substitute the Zr atoms in the ZrN lattice. Exceeding the solubility limit, a nanocomposite film containing ZrN:Si nanocrystallites surrounded by amorphous SiN_y is formed (Domain 2). Further increase of Si content (Domain 3) implies a reduction of the grain size, while the thickness of the SiN_y layer remains constant at the crystallite surface. The increasing

Corresponding author: R. Sanjines, e-mail: rosendo.sanjines@epfl.ch

© 2007 Advanced Study Center Co. Ltd.

amount of the SiN_y amorphous phase in the films is realized by increasing the surface to volume ratio of the crystallites.

In such nanocomposite thin films (nc-TMN/amorphous-SiN_y), crystallite sizes are of the order of a few nanometers. The grain surfaces and boundaries play an increased role on physical properties. The location, the thickness and the chemical composition of the amorphous minoritary SiN_y phase are crucial for electrical properties [8,9]. It has been shown that the electrical resistivity measured as a function of temperature provides experimental means for following the thickness evolution of the SiN_y coverage layer in such nanocomposite films [9].

Since the phase segregation is diffusion-controlled [11], the deposition temperature is a key parameter for controlling the thickness of the SiN_y coverage layer. For this purpose series of Zr-Si-N films with various Si content were deposited at various substrate temperatures: RT, 240, 440, and 640 °C. In order to understanding the effect of the phase segregation on the formation of the composite material, the optical and electrical properties of Zr-Si-N films were investigated by spectroscopic ellipsometry and electrical resistivity measurements.

2. EXPERIMENTAL

The deposition of Zr-Si-N films was carried out by DC reactive magnetron sputtering of Zr and Si targets in Ar + N_2 atmosphere. The residual pressure in the reactor was less than $3 \cdot 10^{-5}$ Pa. During the deposition, the total pressure was kept constant at 0.5 Pa for all Zr-Si-N films. Four series of samples have been deposited at various substrate temperatures T_S: room temperature (RT), 240 °C, 440 °C, and 640 °C. Depending on T_S, different N_2 partial pressures are required for obtaining nearly stoichiometric ZrN films. The nitrogen partial pressure was kept constant for each series at 5%, 12.5%, 37.5%, and 65%, respectively. The power applied on the Zr target was 100 W, whereas the power on the Si target was varied between 10 and 100 W. The target diameters were 5 cm. The substrates were polished silicon wafers and oxidized silicon wafers. The film thicknesses, measured by profilometry, were between 0.9-1.2 μm. The chemical composition was obtained by electron probe microanalysis (EPMA) [10]. Electrical resistivity was measured by the van der Pauw method in a temperature range between 300K and 20K. The ellipsometric measurements were performed in the photon energy range of 0.75 – 5.0 eV using an Uvisel Jobin-Yvon ellipsometer (at 70°). The Zr-Si-N films are optically opaque in the Si compositional range studied.

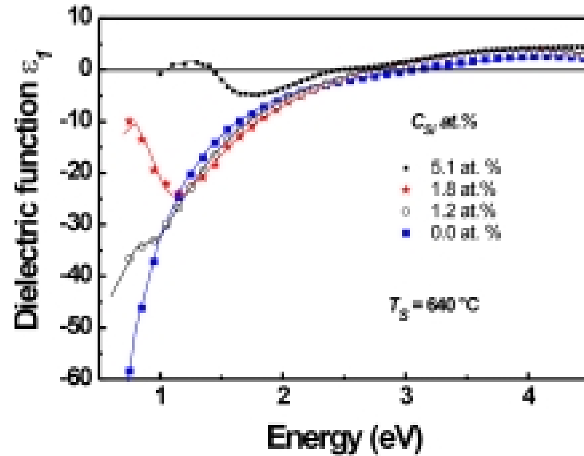

Fig. 1. Real part of the dielectric function ε_1 fitted (solid line) with the Drude-Lorentz model for ZrN and Zr-Si-N thin films with four Si contents.

3. RESULTS

3.1 Optical properties

Values of the real and imaginary parts of the dielectric function $\varepsilon(\hbar\omega) = \varepsilon_1 + i\varepsilon_2$ were obtained from ellipsometric measurements. With increasing the Si content in the films, the general trend of ε_1 and ε_2 is the change from metallic to dielectric like behaviour. Typical spectra of real part of dielectric function ε_1 for ZrN and Zr-Si-N films with C_{Si} = 1.2, 1.8, and 5.1 at.% deposited at 640 °C are shown in Fig. 1. For films having low Si content $C_{Si} \leq 4$ at.%, the values of the screened plasma energy $\hbar\omega_{ps}$(defined as the light energy for which $\varepsilon_1 = 0$) change little in comparison with that observed in pure cubic ZrN films ($\hbar\omega_{ps}$= 3.2±0.1 eV). However, it decreases from 3.2±0.1 eV to 1.5 ±0.1 eV with increasing C_{Si} to about 5 at.%. For higher Si content, the films have a dielectric behavior. The Si addition leads to the presence of an absorption band at ~1 eV (Fig. 1). For C_{Si} > 1 at.% an oscillator with a resonance photon energy $\hbar\omega$ = 0.8-1.5 eV has to be introduced to provide the observed

Table 1. Representative values of the fitted Drude-Lorentz parameters for Zr-Si-N films. Three Lorentz oscillators located at 2.4-2.6 eV, 4.0-4.5 eV, and 6.0-6.5 eV have been introduced to account for interband transitions at the Γ and X points of the Brillouin zone [9].

Deposition temperature : RT			Deposition temperature: 240 °C		
Si at.%	$\hbar\omega_p$(eV)	Γ(eV)	Si at.%	$\hbar\omega_p$(eV)	Γ(eV)
0	5	1.8	0	6.6	0.6
1.48	5.4	1.5	0.82	6.8	0.4
3.44	5.5	1.55	1.6	6.2	0.8
5.1	7	2.3	2.4	6.6	1
7.2	7	2.3	3.78	6.3	1
9.3	7	2.6	4.4	6.1	1.2
			5.33	5.7	1.9
Deposition temperature : 440 °C			**Deposition temperature: 640 °C**		
Si at.%	$\hbar\omega_p$(eV)	Γ(eV)	Si at.%	$\hbar\omega_p$ (eV)	Γ(eV)
0	5.7	0.72	0	6.3	0.3
0.55	5.4	0.3	0.35	6.6	0.28
1.2	7	0.6	0.56	7.3	0.3
1.54	6.2	0.3	1.2	6.6	0.55
2.62	6.6	0.8	1.55	6.2	0.7
3.84	6.4	1.4	1.81	6.2	0.7
4.74	5.4	1.65	2.56	6.4	0.8
			3.41	6.4	0.85
			5.11	6.3	1.15

dispersion of the dielectric function. The position and the intensity of this absorption peak are correlated with the Si content in the films.

In order to have an insight in the compositional dependence of the free carrier density, the plasma frequency ω_p and the damping factor Γ_p have been computed from the ellipsometric measurements. Following the analysis procedure describe in Refs [9,12] the dielectric function spectra were fitted under the assumption that the intra-band and inter-band transitions can be described by a Drude term and a set of Lorentz oscillators, respectively. The plasma frequency is related to the effective optical free electron density and given by the relation

$$N^* = N\frac{m_e}{m^*} = \frac{\varepsilon_0 m_e \omega_p^2}{e^2}, \quad (1)$$

where m_e is the mass of the electron and e the electron charge. Γ_p is related to the charge carrier scattering time τ_p by $\Gamma_p = \hbar/\tau_p$. As resulting from Table 1 and Fig. 2, the charge carrier scattering time τ_p appears to be the significant parameter in the description of the influence of the Si content on the optical properties of the Zr-Si-N films. The smallest values of $\Gamma p \approx 0.3$ - 0.7 eV are observed in the Zr-Si-N films deposited at 440 and 640 °C with (CSi) < 3 at.% and correspond to the charge carrier scat

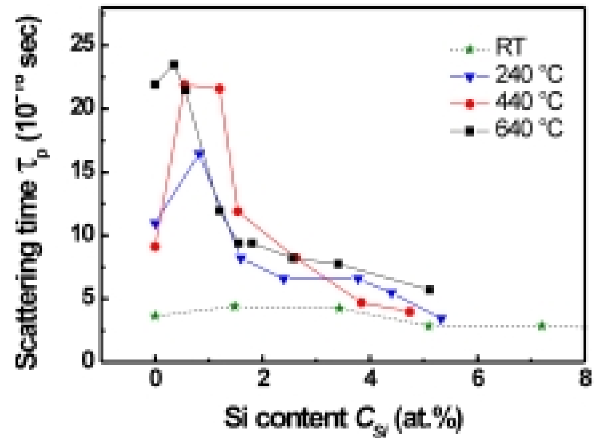

Fig. 2. Charge carrier scattering time τ_p obtained by fitting the data with the Drude-Lorentz model for Zr-Si-N films as a function of the Si content and substrate temperature.

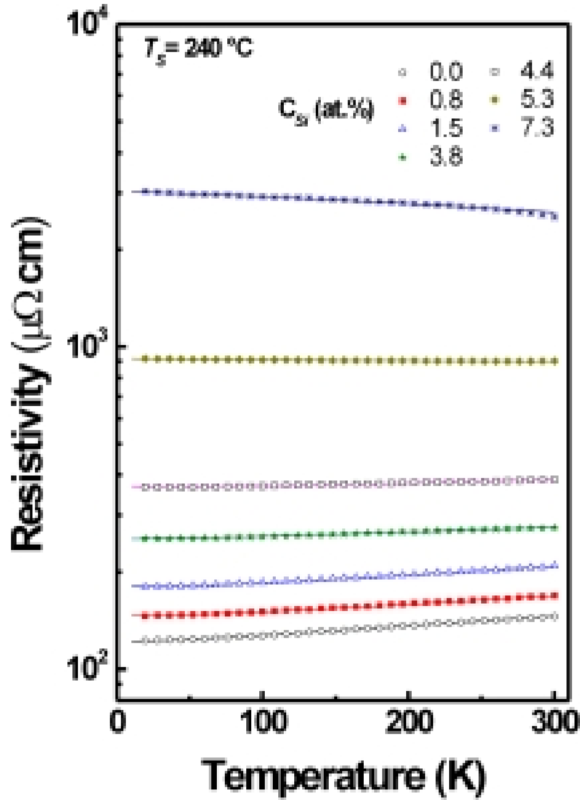

Fig. 3. Zr-Si-N thin films deposited at 240 °C: electrical resistivity ρ *vs.* temperature *T* for various Si concentration C_{Si} in at.%. The solid lines are the best fitting with the grain boundary model.

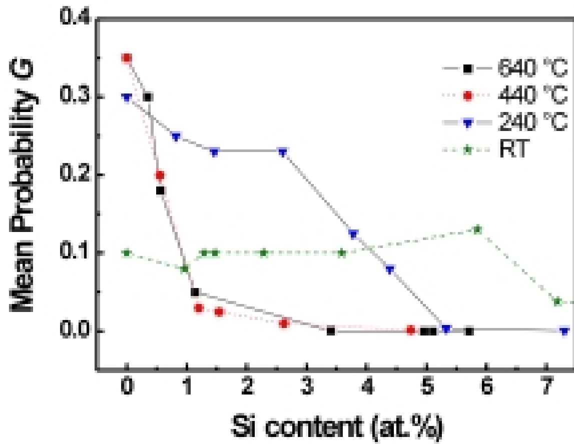

Fig. 4. Grain boundary transmission probability *G* as a function of the Si content for Zr-Si-N thin films deposited at RT, 240, 440, and 640 °C.

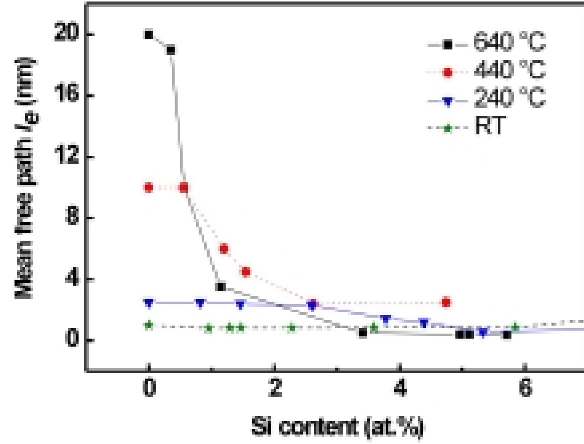

Fig. 5. Elastic scattering mean free path l_e as a function of the Si content for Zr-Si-N films deposited at RT, 240, 440, and 640 °C.

tering time $\tau_p \approx$ (22- 8.2) 10^{-16} s. These values are similar to those observed in large grain size crystallized nitrides (20-30 nm). At higher Si content, the Γ_p (0.8-1.2 eV) values are comparable to those reported for fine grain size polycrystalline nitrides (10-15 nm) [9,12]. Films deposited at RT are most prone to have a large plasma damping factor (between 1.5 to 2.6 eV) because they have highly disordered crystal structure and small crystallites as reported in [10].

3.2 Electrical properties

Typical temperature dependant d.c. electrical resistivity curves of the Zr-Si-N films as a function of Si content (C_{Si}) are shown in Fig. 3 for films deposited at 240 °C. Films deposited at RT, 440, and 640 °C exhibit similar behavior. The resistivity ρ(*T*) of Zr-Si-N films with $C_{Si} < 5$ at. % exhibits metallic behavior while those having $C_{Si} > 5$ at.% exhibits a negative temperature coefficient of resistivity (TCR $=1/\rho\cdot\partial\rho/\partial T$). This anomalous normal resistivity is explained in terms of grain boundary scattering effects or electron localization in weakly disordered metallic materials (weak localization model)[13-16]. The transport mechanism in the Zr-Si-N thin films is well described by the grain boundary scattering model. According to grain boundary scattering model, the dc electrical resistivity is given by

$$\rho_g = \left(\frac{m_e^* \nu_F}{Ne^2}\right)\left(\frac{1}{L}\right)G^{-(L/D)} = \left(\frac{K}{L}\right)G^{-(L/D)}, \qquad (2)$$

where m_e^* is the effective masse of the charge carriers, ν_F is the Fermi velocity, *N* is the density of the

Table 2. Typical parameters obtained for the best fit of the electrical resistivity of Zr-Si-N thin films with the grain boundary scattering model

Deposition temperature : RT			Deposition temperature: 240 °C		
Si at.%	Probability G	Mean free path l_e (nm)	Si at.%	Probability G	Mean free path l_e (nm)
0	0.1	1	0	0.3	2.5
0.96	0.08	0.8	0.82	0.25	2.5
1.29	0.1	0.83	1.46	0.23	2.4
1.47	0.1	0.83	2.6	0.23	2.3
2.28	0.1	0.83	3.78	0.125	1.44
3.59	0.1	0.85	4.39	0.08	1.2
5.85	0.13	0.85	5.33	0.0037	0.55
7.18	0.038	1.4	7.3	0.0008	0.75
9.49	0.026	1.3			
Deposition temperature : 440 °C			Deposition temperature: 640 °C		
Si at.%	Probability G	Mean free path l_e (nm)	Si at.%	Probability G	Mean free path l_e (nm)
0	0.35	10	0	0.35	20
0.55	0.2	10	0.35	0.3	19
1.2	0.03	6	0.56	0.18	10
1.54	0.025	4.5	1.14	0.05	3.5
2.62	0.01	2.4	3.41	0.00025	0.5
4.74	0.0015	2.5	4.96	0.000015	0.4
			5.11	0.00009	0.4
			5.71	0.00005	0.38

charge carriers, D is the average grain size, L is the inner-crystalline mean free path and G is the mean probability for electrons to pass a single grain boundary [13]. In this model, an effective mean free path $L_G = LG^{(L/D)}$ is introduced to describe the electron scattering including the grain size effect. The inner-crystalline mean free path L, describing the volume scattering of electrons, is limited by a temperature invariant elastic scattering at lattice defects and acoustic phonons, namely l_e, and by the temperature dependant inelastic scattering, l_{in}, $L^{-1} = l_e^{-1} + l_{in}^{-1}$. The inelastic mean free path is approximated by $l_{in} \approx \alpha T^{-p}$ where α and p are material specific constants [16]. For the theoretical modeling via the relation (2) we assumed $K = \left(m_e^* v_F / Ne^2\right) \approx$ (10-20) 10^{-6} $\mu\Omega cm^2$ (using $N \approx$ (1-4) 10^{22} cm^{-3} and $v_F \approx 1.0\ 10^8$ cm s^{-1} as deduced from optical measurements). In the case of films deposited at 240 °C, the best fitting using the model are shown in Fig. 3 as continuous lines for every Zr-Si-N film. For all the investigated films, the representative values of the fitting parameters are listed in Table 2.

The parameters reported in Table 2 suggest that, depending on the Si content, the transport properties of the Zr-Si-N films exhibit two different regimes of grain boundary scattering: one regime of relatively high electron transmission probability $0.1 \leq G \leq 0.35$ and another regime of low probability $G < 0.1$. The critical value of the Si content at which the transition from the former to the latter regime occurs depends on the deposition temperature. As shown in Fig 4, for films deposited at 440 and 640 °C a sharp transition is observed at about 1.0 at.% of Si while for films deposited at 240 °C a blunt transition is observed between C_{Si} = 3-5 at.%. In the case of films deposited at RT, the transmission probability G exhibits restrained values of 0.1 - 0.15 and the threshold is observed above C_{Si} = 7 at.%. The second important computed parameter, namely l_e, is shown in Fig. 5 as a function of the Si

content. The elastic scattering free path l_e depends on the Si content and on the deposition temperature. It decreases with increasing Si content.

4. DISCUSSION

The electrical and optical properties of the Zr-Si-N film deposited at RT, 240 °C, 440 °C, and 640°C can be correlated with the microstructural modifications of the Zr-Si-N films due to the diffusion and segregation of Si atoms. As reported in Ref [10], the morphology (crystallite shape, size and orientation) of Zr-Si-N films is extremely sensitive to the addition of Si atoms and the deposition temperature. All Zr-Si-N films exhibits columnar like morphology with crystallites elongated on the growth direction. The increase of Si content leads to decreases of the average crystallite size in Zr-Si-N films.

It is important to point out that by increasing the substrate temperature the solubility limit of Si in ZrN lattice decreases whereas the Si surface coverage increases [10]. The values of the pairs {solubility limit, Si surface coverage} in the Zr-Si-N films are {5%, 0.2}, {4%, 0.5}, {2%, 0.85}, and {1%, 1.8} for RT, 240 °C, 440 °C, and 640 °C, respectively [10]. We observe that the mean probability for electrons to pass the grain boundary *G* is related to the formation of the SiN_y coverage layer. In the films deposited at 440 °C and 640 °C, where the solubility limits are small and the thicknesses of SiN_y grain boundary layer are high, *G* deeply decreases at C_{Si} < 2 at.% (Fig. 4). For the films deposited at RT and 240 °C (with higher solubility and lower thicknesses of SiN_y layer), *G* decreases slowly and at higher C_{Si} (see Fig. 4). The electron scattering mean free path le depends on the lateral crystallite size and on the crystallographic defects density. As it was shown in Ref. [9-11] the rate of the decrease of the grain size ($-\Delta D/\Delta C_{Si}$) depends directly on the Si surface coverage, which increase with increasing the substrate temperature T_S. In Fig. 5, we observe that the rate of decrease of the electron scattering mean free path le ($-\Delta l_e/\Delta C_{Si}$) is higher for higher substrate temperature. We can point out that the evolution of the electron scattering mean free path le with increasing the Si content is well correlated with the evolution of the film morphology (ZrN crystallite size and SiN_y layer thickness).

5. CONCLUSION

The evolution of the Si solubility limit and of the SiN_y coverage layer thickness as a function of Si content and substrate temperature T_S, as deduced from morphological model, are well correlated with the evolution of the electron scattering mean free path l_e and the mean probability for electrons to pass the grain boundary *G*. In this way, electrical and optical measurements are useful techniques for obtaining a complete description of the evolution of the Zr-Si-N films properties with increasing Si content and at various substrate temperatures. They provide experimental mean for following the thickness evolution of the SiN_y boundary layer in the composite films.

REFERENCES

[1] M. Diserens, J. Patscheider and F. Lévy // *Surf. Coat. Technol.* **108–109** (1998) 241.

[2] S. Veprek // *J. Vac. Sci. Technol. A* **17** (1999) 2401.

[3] J. Musil // *Surf. Coat. Technol.* **125** (2000) 322.

[4] M. Benkahoul, C.S. Sandu, N. Tabet, M. Parlinska-Wojtan, A. Karimi and F. Lévy // *Surf. Coat. Technol.* **188-189** (2004) 435.

[5] D. Pilloud, J. F. Pierson, A. P. Marques and A. Cavaleiro // *Surf. Coat. Technol.* **180-181** (2004) 352.

[6] J. H. Park, W. S. Chung. Y-R. Cho and K. H. Kim // *Surf. Coat. Technol.* **188-189** (2004) 425.

[7] M. Nose, W.A. Chiou, M. Zhou, T. Mae and M. Meshii // *J. Vac. Sci. Technol. A* **20** (2002) 823.

[8] C.S. Sandu, M. Benkahoul, R. Sanjinés and F. Lévy // *Surf. Coat. Technol.* (2006) doi:10.1016/j.surfcoat.2006.06.003.

[9] R. Sanjinés, M. Benkahoul, C.S. Sandu and F. Lévy // *J. Appl. Phys.* **98** (2005) 123511.

[10] C.S. Sandu *et al.* // *Surface & Coatings Technology* (2006) doi:10.1016/j.surfcoat.2006.08.002.

[11] C.S. Sandu *et al.* // *Surface & Coatings Technology* (2006) doi:10.1016/j.surfcoat.2006.08.100.

[12] A. Nigro, G. Nobile, M.G. Rubino and R. Vaglio // *Phys. Rev.* **B 37** (1988) 3970.

[13] G. Reiss, J. Vancea and H. Hoffman // *Phys. Rev. Lett.* **56** (1986) 2100.

[14] R. Lamni, E. Martinez, S.G. Springer, R. Sanjinés, P.E. Schmid and F. Lévy // *Thin Solid Films* **447-448** (2004) 316.

[15] M. Kaveh and N.F. Mott // *J. Phys. C: Solid State Phys.* **15** (1982) 707.

[16] J-H Tyan and T. Lue // *J. Appl. Phys.* **75** (1994) 325.